Electrodeposition and Characterization of Hydroxyapatite on TiN/316LSS

Pham Thi Nam, Dai Lam Tran, Thu Huong Ho, Thu Phuong Nguyen, Thi Thu Trang Nguyen, Thai Hoang, Thi Thanh Huong Nguyen, Ba Thang Le, Christophe Drouet, David Grossin, et al.

Electrodeposition and Characterization of Hydroxyapatite on TiN/316LSS

Pham Thi Nam[1], Tran Dai Lam[2], Ho Thu Huong[1], Nguyen Thu Phuong[1], Nguyen Thi Thu Trang[1], Thai Hoang[1], Nguyen Thi Thanh Huong[1], Le Ba Thang[1], Christophe Drouet[3], David Grossin[3], Emmanuelle Kergourlay[3], Ghislaine Bertrand[3], Didier Devilliers[4], and Dinh Thi Mai Thanh[1,*]

[1]*Institute for Tropical Technology,*
[2]*Institute of Materials Science, Vietnam Academy of Science and Technology, 18 Hoang Quoc Viet Street, Cau Giay, Ha noi, Vietnam*
[3]*CIRIMAT Carnot Institute, UMR CNRS/UPS/INPT 5085, University of Toulouse, ENSIACET, 4 allée Emile Manso, 31030 Toulouse cedex 4, France*
[4]*Sorbonne Université, UPMC, UMR CNRS PHENIX 8234, Paris, France*

The deposition of TiN on stainless steel substrates may improve the stability and compatibility of this material with bone, which may be advantageously exploited for the elaboration of advanced prosthetic devices. ln this work, TiN-coated 316LSS (by way of DC magnetron sputtering) was used as a starting material for investigating the electrochemical post-deposition of hydroxyapatite (HAp) which has a composition close Io that of bone. Electrodeposition was carried out starting from an aqueous medium containing solubilized $Ca(N0_3)_2$ and $NH_4H_2P0_4$ in the presence of H_20_2. We report the influence of experimental conditions on the morphology of the obtained HAp coating on TiN/316LSS. The effect of applied potential, temperature, H_20_2 concentration, pH and duration of reaction were thoroughly discussed on the basis of X-ray diffraction (XRD), scanning electron microscopy (SEM), Fourier Transform lnfrared (FTIR) spectroscopy and Energy Dispersive X-ray Spectroscopy (EDX) results. This method appears advantageous for producing HAp-coated implant materials.

Keywords: Titanium Nitride (TiN), 316L Stainless Steel (316LSS), Hydroxyapatite (HAp), Coating, Electrodeposition.

1. INTRODUCTION

Titanium and Ti-based compounds have excellent properties such as good corrosion resistance in extreme conditions, high strength-to-density ratio and low toxicity. These properties together with an intrinsic biocompatibility are exploited in a variety of medical applications such as orthopedic and osteosynthesis devices, dental implants, maxillo-facial surgery and vascular stents.[1,2] However, in some implant cases, they do not forrn strong chemical bonds with natural bones.[3-5] A great deal of research projects are undergone worldwide with the view to further improve the osteointegration of such metal implant materials and favor bone tissue growth.[6,7] Among envisioned strategies, the coating of implants by hydroxyapatite (HAp, $Ca_{10}(P0_4MOH)_2$), is particularly prornising. HAp has indeed a chernical composition close to that of the minerai component of natural bone and may accelerate bone growth onto the surface of implant during the early stages after implantation.[8] HAp has thus been widely used as a coating material for dental and orthopedic implants for many years.[2,9,10]

Nevertheless a variety of technologies for coating HAp onto bio-medical metal surfaces have been developed. They included pulsed laser deposition,[11,12] plasma spraying,[13-15] ion beam sputtering,[16] sol-gel,[17] electrophoretic deposition,[18] and electrochemical deposition.[2,4,19,20] In recent years, the electrochemical deposition of HAp on metal or alloy surfaces has become technologically important for various applications.[2]

In the present study, the influence of experimental conditions (such as H_20_2 content, applied potential, temperature, pH and reaction time) on the electrodeposition

*Author to whom correspondence should be addressed.

of HAp on TiN/316LSS substrate was investigated. The morphology, structure and composition of the coating were thoroughly characterized by X-ray diffraction (XRD), Field-Emission Scanning Electron Microscopy (FE-SEM), and Fourier transform infrared (FTIR) spectroscopy.

2. MATERIALS AND METHODS

2.1. Preparation of TiN/316LSS Substrates

TiN-coated 316LSS substrates were obtained via DC magnetron sputtering. Typical samples had the following dimensions: 100 x 10 x 2 mm, corresponding to a working area of 1 cm² (surrounded by epoxy resin). The TiN film has thickness about 1 μ,m with single-phase crystal and spherical shape with a diameter about 5-10 nm (Fig. 1).[21]

2.2. Preparation and Characterization of HAp Coating

HAp coating on the TiN/316LSS substrate was performed electrochemically in solution S containing 3 x 10-² M $Ca(N0_3)z$ (aq) and 1.8 x 10-2 M $NH_4H_2P0_4$ (aq), leading to a Ca/P molar ratio in solution identical to that of stoichiometric hydroxyapatite (1.67). The initial pH of electrolytes was 4.5 and was adjusted to increase or decrease by a solution of 1 M NH_40H or 1 M $HN0_3$. 0.15 M $NaN0_3$ (aq) was added, mainly to increase the ionic strength of the electrolyte and also to potentially use the electrochemical reduction of N03 ions contributing to generate a local alkaline environment through the generation of oH- ions.[19] $x\,o/o$ H202 (with $x = 0$, 2, 4 and 6%, w/w) were also added to the electrolyte so as to provide an alternative electrochemical source of hydroxide ions at the substrate (cathode) surface, thus favoring HAp formation, without the need to generate hydrogen that can damage the film.[20]

The electrodeposition was carried out with an AUTOLAB potentiostat using different cathodic potentials -1.5, -1.6, -1.65, -1.7 and -1.8 V/SCE. Different deposition times were investigated, namely 30, 45, 60, 75 and 90 minutes as well as solution pH values ranging from 4.0 to 5.5 (the solution pH was measured with a precise Radiometer analytical pH meter). Different reaction temperatures were studied: 25, 40, 50, 60; 70 and 80 °C (the temperature was maintained constant by a thermostat, model NNT-2400, Eyel). The electrochemical cell contained 80 ml electrolyte. A linear polarization method with potential ranging from equilibrium potential to -2.5 V/SCE was used to deterrnine the reduction potential of reactions occurring on the TiN/316LSS electrode. After deposition, the specimens were rinsed with distilled water to remove residual electrolyte, then incubated at 25 °C for 24 h for further analyses. The mass of HAp formation on TiN/316LSS surface was deterrnined using a Precisa XR 205 SM-DR analysis balance.

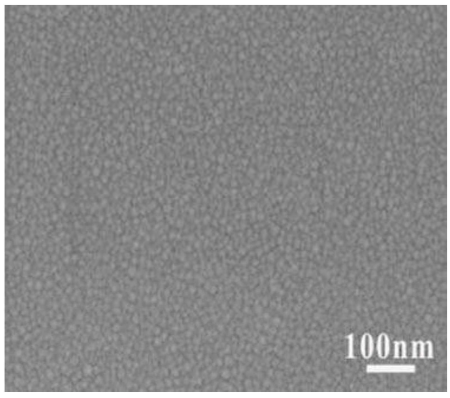

Figure 1. FE-SEM image of TiN coating.

The surface morphology and composition of the coating were studied with Hitachi S-4800 FE-SEM equipped with an Energy-Dispersive X-ray (EDX) analyzer. XRD patterns were recorded with a Siemens D5000 diffractometer using CuK" radiation (À = 1.54056 Â) with a step angle of 0.03°, a scanning rate of 0.04285°-ç¹ in the *28* range 10--70°.

HAp has a hexagonal lattice system with $a = b\#c$, $a = f3 = 90°$, $y = 120$ °C. XRD can determine the value of the distance between the crystal planes (d), changing the value of d in Eq. (1) to deterrnine the a and c parameters.

$$\frac{1}{d2} = \frac{4/3(h^2 + kh + k^2)}{a2} + \frac{1^2}{c2} \quad (1)$$

Where h, k, l are (hkl) indices of the peaks of HAp

FTIR spectra were recorded with a Nicolet 6700 spectrometer, using the KBr pellet technique[22] in the range of 4000--400 cm-¹, with a resolution of 8 cm-¹. Ail measurements were performed at room temperature after incubated at 25 °C for 24 hours.

3. RESULTS AND DISCUSSION

3.1. Effect of H_20_2 Concentration

The concentration of H_2O_2 was previously shown to influence the formation of HAp on 316LSS,[2] so it was judged interesting in this study to investigate also this phenomenon on TiN/316LSS. Moreover, to our knowledge, there has not been much research on this subject in literature. For exploring this effect, the preparation of HAp was carried out by cathodic polarization. This method always occurs in parallel with the reduction of water which releases H_2 and consumes a large quantity of electric energy, decreasing the formation yield of Pol- and OH- ions, and decreasing in turn the amount of generated HAp. Furthermore, the generated H_2 gaseous bubbles make HAp coating more porous and Jess adhesive to the substrate surface. In order to overcome these drawbacks, H_20_2 is often added into the synthesis solution due to its strong oxidizing power, instead of pure water. For the fabrication of HAp, the presence of H_20_2 is clearly advantageous as it

is reduced a1 the cathode to generate OH- ions after the following equation (Eq. (2)).[23,24]

$$H_2O_2 + 2e^- = 2OH^- \quad (2)$$

The cathodic polarization method was used to investigate the effect of the concentration in $Hz0_2$ on the formation of HAp on TiN/316LSS in solution S. Various concentrations of $Hz0_2$ (0%; 2%; 4%; 6%) in S were studied and the cathodic polarization curves were recorded with predetermined potential scanning from the equilibrium potential down to -2.5 V/SCE, at 25 •C, with a scanning rate of 5 mV/s.

Figure 2(a) shows that, in the potential range from 0 to -0.5 V/SCE, the current density was constant and approximately zero as no reduction reaction occurred. In the potential range from -0.7 to -1.5 V/SCE, the current density slightly increased, corresponding to the reduction of H+ and O_2 dissolved in water. When the potential was lower than -1.5 V/SCE, the current density increased rapidly, resulting from the reduction of HzP04 and water.[2,25]

The formation of HAp on the surface of the cathode was observed. This phenomenon may be explained as follows: when oH- ions were generated on the cathode surface, the pH at the vicinity of the cathode significantly increased in range from 8 to 12, leading to the formation of – and – ions, these ions then reacted with Ca2+ ions to form HAp coating according to Ilqs. (3}-{5).

$$H_2P04 + OH- \text{ --. } HPD;- + H20 \quad (3)$$

$$HPD;- + oH- \text{ --. } ro:- + HzO \quad (4)$$

$$10Ca^{2+} + 6PO_4 - + 20W \text{ --. } Ca_{10}(P0_4MOHh \quad (5)$$

Figure 2(b) presents the variation of the current density versus the duration of the HAp electrodeposition process on TiN/316LSS at -1.65 V/SCE and 25 °C, with Hz02 concentration varying between 0 and 6%. The appearance of the different curves is similar and two major zones can be distinguished. For the first one, the current density increased suddenly, corresponding to the double layer accumulation of H_2P04 ions on the cathode, then the current density decreased due to an effect of diffusion. For the second one, the current density stabilized, corresponding to the HAp synthesis process. When $Ilz0_2$ concentration increased from O to 6%, the cathode current density also increased from about 9.5 to 11.5 mA·cm^{-2}.

However, the highest $Hz0_2$ concentration (6%) induced a significant increase of the amount of OH- ions around the cathode, therefore HAp was not only formed on the electrode surface but also in the solution in the cathode region: for this concentration, the white HAp powder was observed and precipitated in the electrochemical cell.

Even at lower H_20_2 concentrations in solution, this compound induced an increase of the concentration of OH- around the cathode surface that affected significantly the formation of HAp. A morphology analysis of HAp coating synthesized at -1.65 V/SCE with H_20_2 concentration range of 0-6% was conducted. SEM images pointed out a clear change of the shape (Fig. 3) and size of precipitated crystals (Table I). Without $Hz0_2$ in solution, the coating exhibited a rod-like structure with sizes from 100 nm to 150 nm (Fig. 3(a)). When $Hz0_2$ was present in the solution, the crystal shape varied significantly. At $Hz02$ concentration of 2-4%, the coating presented a porous structure with a flake-like shape (Figs. 3(b) and (c)). It was difficult to determine precisely the crystal dimensions in these cases. At H_20_2 concentration of 6%, the crystals had a spherical shape with rather heterogeneous sizes varying from 60 to 400 nm. These results are summarized in Table I. It is noted that the crystal morphology obtained with 4% $Hz0_2$ concentration was similar to the shape of HAp crystals formed in simulated body fluids (SBF) solution.[2] This H_20_2 concentration of 4% was thus considered as "optimized" for obtaining such a coating in the conditions of this work.

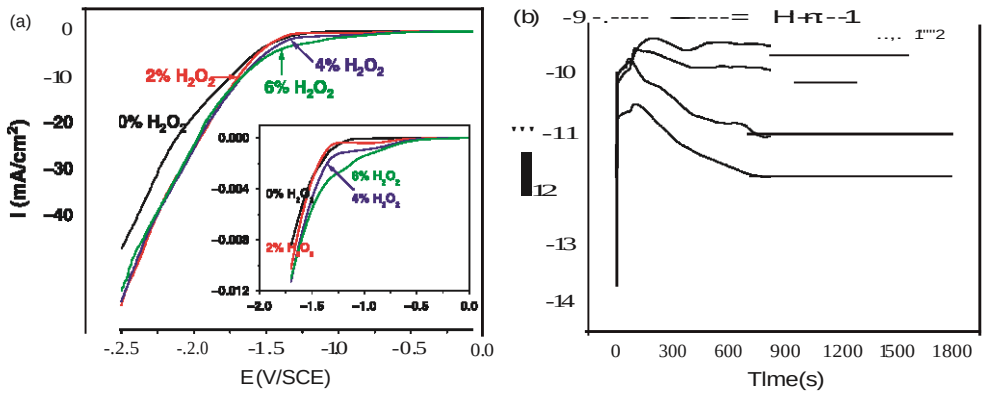

Figure 2. Cathodic polarization curves of TiN/3161.SS electrode with various concentration of Oz; (b) Variation of the current density during the HAp formation on TiN/3161.SS at -1.65 V/SCB, for various 0_2 concenttations.

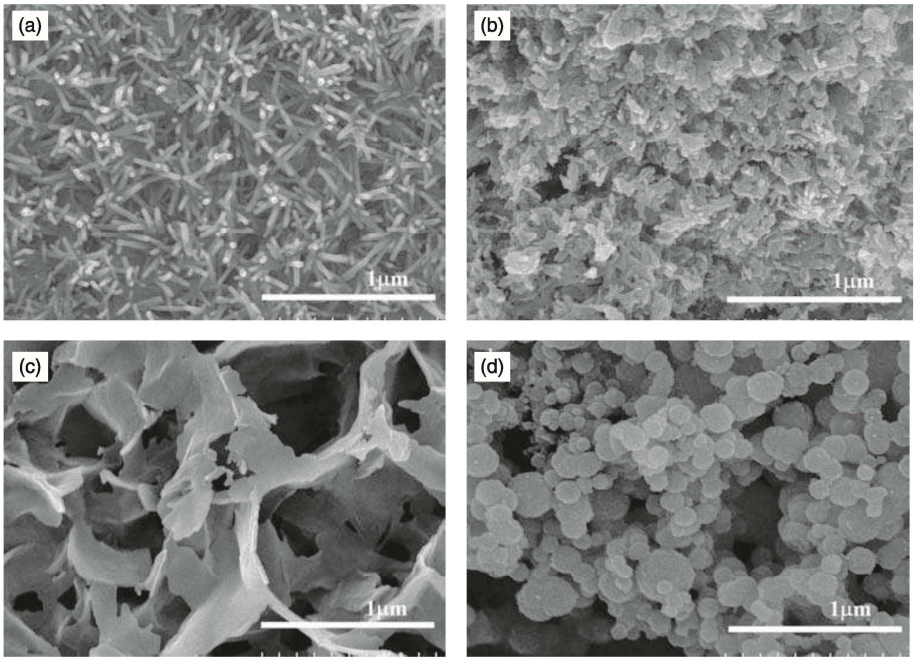

Figure 3. SEM images of the HAp fonned in solution S; pH 4.5; applied potential -1.65 V/SCE; 25 °C; with various H_2O_2 concentrations (a) 0%; (b) 2%; (c) 4% and (d) 6%.

3.2. Effect of the Synthesis Potential

The potential applied is bound to directly influence the formation of OH- ions, and thus of the HAp coating. Various values of potential (from -1.5 to -1.8 V/SCE) were thus checked here to study the effect of this parameter, using solution S, 4% H_2O_2, total duration: 30 minutes, at 25 °C. The variation of current density versus time at different values of potential is shown in Figure 4. The current density increases followed by stabilization that relates to the growth of HAp on the surface of electrode. When cathodic applied potential decreased from -1.5 to -1.8 V/SCE, the cathodic current density increased from 5 to 18 mA $\cdot cm^{-2}$. The formation of white HAp coating on the TiN/316LSS electrode surfaces was observed. However, when the applied cathodic potential was more negative than -1.65 V/SCE, the adhesion strength of HAp on the substrate was poor and particles were released in the solution.

The related HAp morphologies were also analyzed. Figure 5 and Table II present the change in morphology and size of the HAp formed on TiN/316LSS electrode at the different values of potential. The HAp surface morphology can be divided in two categories: type 1 corresponded to the potential values -1.5, -1.6, -1.65 V/SCE, for which the HAp crystals formed on TiN/316LSS surface had a flake shape with sizes difficult to assess. Type II corresponded to the applied potential at -1.7 and -1.8 V/SCE, for which the HAp crystals had a spherical shape with sizes varying from 40 to 300 nm. When the applied cathodic potential decreases, the OH- formation near the cathode increases, causing the increase of the rate of HAp crystal growth and the change of HAp

Table 1. Morphology and size of HAp crystals synthesized at various H_2O_2 concentrations from 0 to 6%.

H_2O_2 concentration (%)	0	2	4	6
HAp crystal shape	Rod	Flake	Flake	Spherical
Size range (nm)	100-150	Difficult to determine	Difficult to determine	60-400

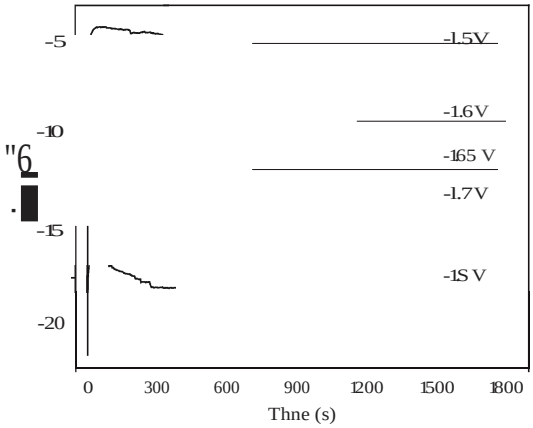

Figure 4. Variation of the current density of the HAp deposition process on TiN/316LSS in solution S; pH 4.5; 25 'C; with various applied potential values from -1.5 to -1.8 V/SCE.

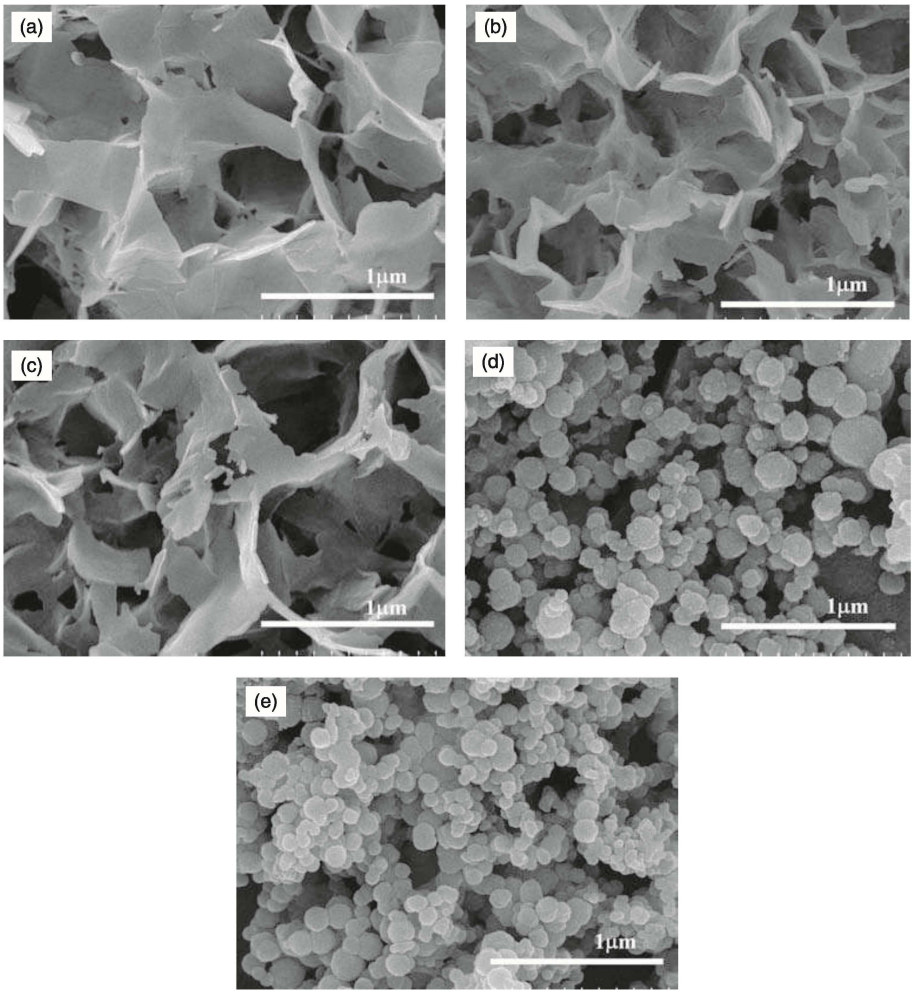

Figure S. SEM images of HAp formed in solution S and 4% H_2O_2 concentration, pH 4.5, 25 'C with various applied potentials: (a) -1.5; (b) -1.6; (c) -1.65; (d) -1.7 and (e) -1.8 V/SCE

morphology. The shape of HAp crystals obtained at the lowest cathodic applied potentials (-1.7 and -1.8 V/SCE) was sirnilar to that of HAp synthesized in the solution containing 6% H_2O_2 concentration. When decreasing the cathodic potential, the reduction of the solvent is promoted, thus the formation of hydrogen bubbles that may induce a spherical shape for the HAp crystals formed. In view of bone-related applications, the cathodic potential range was chosen greater or equal to -1.65 V/SCE which leads to a morphology sirnilar to the shape of HAp formed in simulated body fluid.[2]

3.3. Effect of Temperature

The kinetics of chernical processes is generally affected by the reaction temperature. Unsurprisingly, in electrochemical reactions the formation of substances on the electrode surface is also bound to be affected by temperature. The variation of the current density according to the HAp deposition time in solution S with 4% H_2O_2, pH 4.5, applied potential -1.65 V/SCE at various temperatures is shown in Figure 6(a). The variation of current density versus time presented the same shape and characteristics as previously in Figure 2(b). The current

Table II. Morphology and size of HAp crystals synthesized at various values of potential from -1.5 V to -1.8 V.

E (V/SCE)	-1,5	-1,6	-1,65	-1,7	-1,8
HAp crystal shape	Flake	Flake	Flake	Spherical	Spherical
Size range (nm)	Difficult to determine	Difficult to deterrnine	Difficult to determine	40-300	50-200

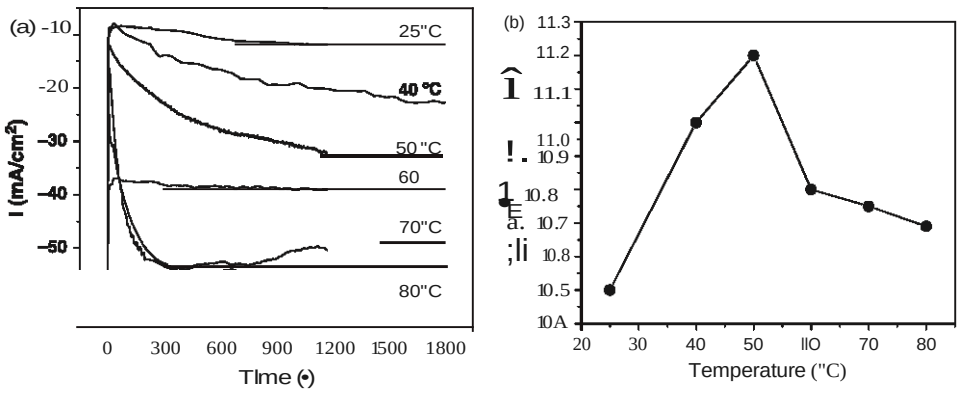

Figunl 6. (a) Variation of the cum:nt density according to the electrodeposition durati.on at wrious temperatures from 25 •C to 80 •C; (b) Variation of the HAp's mass venus temperature.

density and the temperature varied in the sa.me direction, the current density corresponding to the synthesis process increased in a range of 10-55 mAJcm.[2], therefore, the electric charge passing through the cell increased, inducing the rise of the mass of HAp formed on the substrate. However, in the synthesis process, it could be visually observed that the amount of detached HAp particles dropping in the solution also increased with the temperature. Therefore, it could be predicted that the amount of HAp formed on the substrate did not monotonously increase with temperature. To confirm this point. we determined the amount of HAp coating formed on TiN/316LSS by a mass analysis. Figure 6(b) shows the variation of the quantity of HAp formed on TiN/316LSS electrode surface versus temperature. Wh.en the temperature increases up to 50 •C, the amount of HAp coating increased and attained the maximum value around 50 •C. In contrast. when the temperature continued to increase to 80 •C, the amount of HAp diminished. This result was in agreement with the flaking phenomenon observed. The movement of ions varies with the temperature. An increase in temperature causes an increase in the rate of the movement of the ions that promote the coating formation on the electrode surface. However, when temperature becomes too high (greater than 50 °C), the further increase in the amount of OH^- and – allowed also the formation of HAp directly in the solution through the chemical reaction given in Eq. (5). The temperature of 50 •C thus appears as a limit for the increase in coating amount in these working conditions.

In order to investigate the effect of temperature on the HAp features, IR spectra were recorded in wavenumber range 4000-400 cm^{-1}. Figure 7 shows in particular the IR spectra of HAp coatings obtained at 25, 40, 50, 60, 70 and 80 •C. The spectra all indicated the usual vibrational signature of moderately-crystallized calcium phosphate apatites.[26] In particular the asymmetric stretching vibration of P--0 bond was characterized by a band located at 1040 cm^{-1} ($P_3(PO_4)$ mode). The $viPO_4$) asymmetric O-P--0 bending mode was also noticeable (by way of two maxima around 610 and 569 cm^{-1}). Absorption at 3572 and 632 cm^{-1} usually assigned to the 0-H stretching vibration in hydroxyapatite were not clearly distinguished on these spectra. This can probably be explained by the nonstoichiometry of the apatite phase, with a deficiency in calcium and hydroxide groups. Water bands were visible by a large band in the range 3000-3600 cm^{-1} (0-H stretching from water molecules) and by the H-0-H bending band at 1640 cm^{-1}. The association of water molecules with apatite is not surprising, especially for nonstoichiometric apatites which exhibit a hydrated layer on the surface of their constitutive crystals, the extent of which is dependent on synthesis conditions.[27] IR spectra also indicate the presence of some degree of carbonation (arising from atmospheric $C0_2$) associated to the apatite phase, by the presence of contributions in the regions 840-900 and 1350--1550 cm^{-1} respectively assignable to the vibration modes $v_2(C0_3)$ and $P_3(C0_3)$. The narrow peak detected with varying intensities at 1373 crn^{-1} is due to nitrate residues not eliminated during the washing step. Such vibrational characteristics are globally similar to those of the mineral phase of bone and in agreement with XRD studies.

The HAp crystal shape was examined for the various temperatures tested, and Figure 8 shows the corresponding SEM micrographs. HAp morphology was somewhat affected by temperature. At 25 •C, HAp showed a fl.ake shape with a typical size difficult to determine. At 40 °C, petal-like shape was observed with apparent dimensions smaller than at 25 •C. At temperatures 50, 60, 70 °C, the HAp morphology became needle-like with homogeneous size and crystal length in a range of 100-200 nm and some fl.ower-like arrangements can be observed. At 80 °C, HAp petal-like morphology was similar to the one observed at 25 °C and 40 °C but seemed to be more porous. Consequently, the HAp morphology was affected by the electrodeposition temperature and 25 or 40 °C

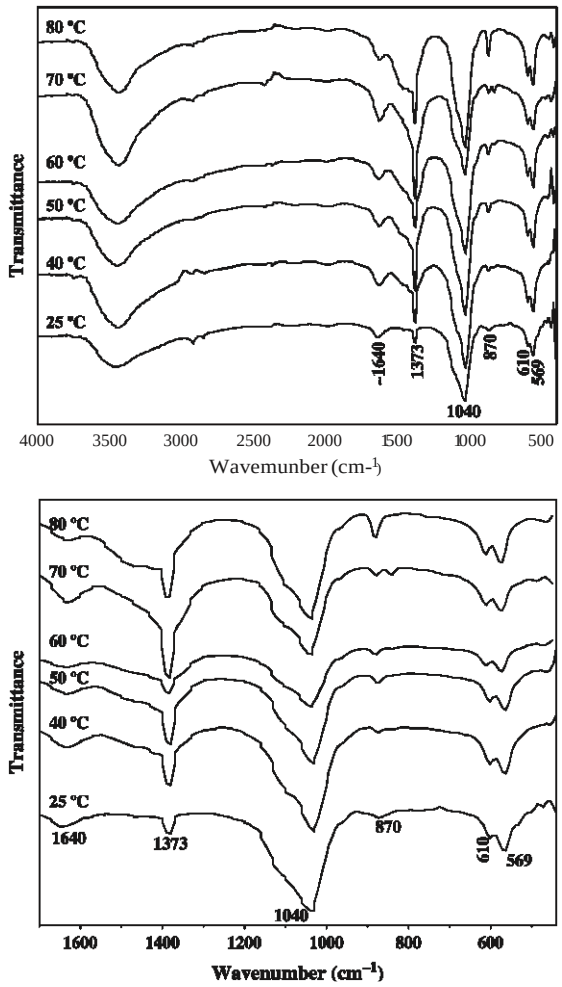

Figure 7. FfIR specil'll of HAp coatings obtairu:d llt vmi.ous tempe.ratures.

appear as favorable testing temperatures, leading to petal-like morphologies often encountered in bone apatite *in vivo*. The peculiar acicular morphology observed at 50, 60 or 70 °C in good agreement with other studies.[23,29] Additional work will be needed in the future to explore further the change at 80 °C and unveil the possible presence of a secondary phase or of a novel morphological settings for hydroxyapatite.

3.4. Effect of pH

Figure 9 shows the current density according to HAp deposition time at the applied potential of -1.65 V/SCE in solution S for various global pH values (remembering that this is not the local pH around the electrode, the alkalinity of which allows the precipitation of apatite): 4, 4.5, *5*, and *5.5*. It is noted that the cathodic current density decreases upon pH increase. This result could tentatively be explained as follows: the OH- concentration increases with the pH increase, inhibiting the reactions generating OH- ions on the cathodic electrode such as the reduction of $l:l:z0_2$, H_2P04 and $l:l:zO$.[2,25] The cathodic current density decreased from 11 mA/cm^2 to 8.5 mA/cm^2 in 1800 seconds with the increase of pH from 4 to *5.5*.

Figure 10 shows SEM images of HAp coating obtained in solution S with various pH values. Ingeneral, the effect of pH value on the HAp morphology was rather insignificant Ail HAp coatings synthesized at various pH values exhibited a flake-like shape.

XRD analyses were run directly on coatings as obtained from electrodeposition in solution S with the previous potential parameters and at various pH values. The results are reported in Figure 11.The XRD patterns showed peaks belonging to a hydroxyapatite-like phase as well as to the TiN/316LSS substrate. Two characteristic peaks of HAp were in particular evidenced at *26* R:: 26° and 32° corresponding to (002) and (211) planes with different peak intensity. Generally, the HAp peak intensity was found to decrease when pH increases. The values of distances between lattice planes and lattice constants of HAp calculated from XRD patterns (Table III) were similar to theoretical values (NIST standard.[30])

Besides, some peaks attributable to dicalcium phosphate dihydrate ($CaHP0_4 \cdot 21:1:z0$, DCPD or brushite) at *26* R:: 29° and 35° corresponding to (14-1) and (060) planes[31] also appear in varying proportions, and DCPD was the major calcium phosphate phase of the films deposited at a pH of *5.5*. This may probably be related to an increased formation of – ions.[25] When pH decreases, the peak intensity of DCPD decreases too. In our experiments, DCPD almost disappeared at pH of 4.5, but it appeared again at pH of 4.0 with a quite strong intensity. Complex interfacial behavior may be at the origin of these rather surprising observations, unless DCPD was also present but could not be detected at pH 4.5. The some peaks of TiN/316LSS substrate also appear in XRD patter with *28* R:: 37° and 45° corresponding to (111) and (200) planes of TIN and *28* R:: 51° corresponding to (200) planes of Fe.[32] At this point, this last pH value for which no DCPD detection was made was however selected as "suitable" for the deposition of HAp on TIN/SS 316L substrate.

3.S. Effect of the Duration of the Polarization

The duration of the process was also investigated in this work. Figure 12 shows the variation of the mass of coating formed on TiN/316LSS in the solution S, 4% $1:1:z0_2$ at 25 °C, pH 4.5, and with an applied potential of -1.65 V/SCE. The weight of coating increased from 10.5 to 12 mg/cm^2 when the duration varied from 30 to 45 minutes. When time continued to increase to 60, 75 and 90 minutes, the mass of coating formed decreased. The formation was maximum with 45 minutes of process and visual observations showed that this duration also corresponded to the most homogenous structure. For short synthesis time, the HAp crystals were formed on the electrode

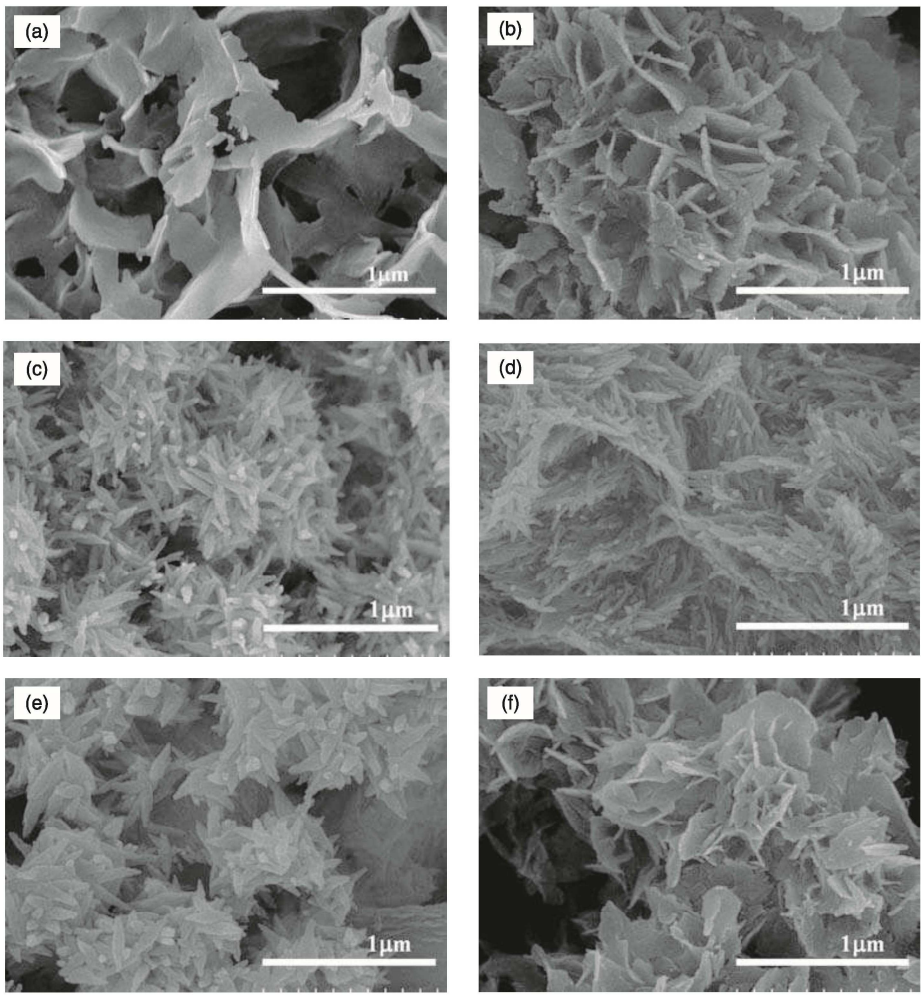

Figure 8. SEM images of HAp formed on TiN/316L SS in solution S, 4% H_2O_2, pH 4.5, applied potential -1.65 V/SCE with various temperatures

W 00 W W WM 00W

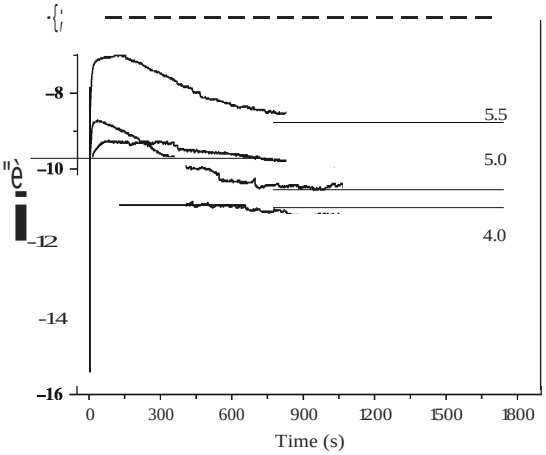

Figure 9. Variation of the current density according to lime inpH range from 4 to 5.5.

by nucleation, and the growth of nucleation increased with time. However, the generated reaction of HAp is the chemical reaction shown in Eq. (5), therefore, the crystallization of HAp on the electrode surface attained the saturation after a certain time. Beyond this stage, the coating loss part of its adhesiveness to the substrate (electrode) surface, and partly dropped into the solution or generated HAp crystallization directly in the solution. This explains the decrease of the amount of HAp measured on the electrode. This result allowed us to evaluate an "optimal" duration for the electrodeposition process of HAp as 45 minutes.

36. Analysis the Chemical Composition of the Coatings

The composition of the coating obtained with the "fully-optimized" electrodeposition conditions was analyzed by EDX method (Fig. 13 and Table IV). The results showed the presence of three main elements that enter in HAp composition: O, Ca, P with contents of 45.08%, 14.31%

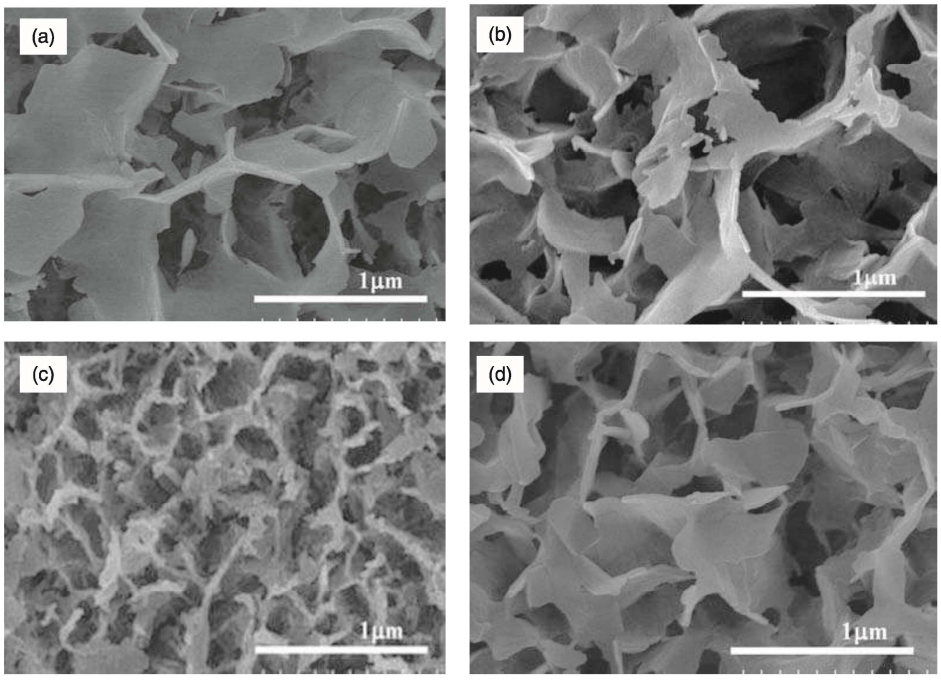

Figure 10. SEM images of HAp formed on TiN/316LSS in solution S. applied potential -1.65 V/SCE at varions pH values: (a) 4.0; (b) 4.5; (c) 5 and (d) 5.5.

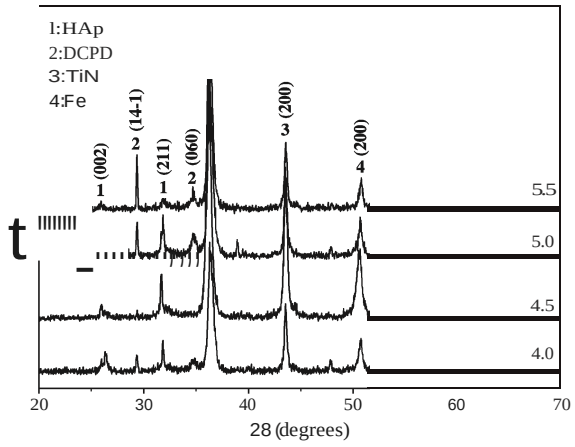

Figure 11. XRD patterns of HAp coatings, obtained by electrodeposition on TiN/SS 316L at different pH values.

Table III. The values of distances (d) between lattice planes with (002) and (211) and lattice constants of HAp according to NIST standard and deposited at pH different.

	Theory (NIST)	pH = 4.0	pH = 4.5	pH = 5.0	pH = 5.5
d(002) (A°)	3.44	3.43	3.44	3.44	3.44
d(211) (A°)	2.82	2.81	2.82	2.81	2.81
a =*b* (A°)	9.41	9.41	9.41	9.41	9.40
C (A°)	6.88	6.86	6.88	6.88	6.88

and 24.92% respectively. Besides, elements such as: Na, Cl, Ti, Cr, Fe and K were also presented. The presence of Na, Cl and K was due to the presence of $NaN0_3$ in the synthesis solution and diffusion of KCl from calomel electrode into the solution. The presence of Ti, Cr and Fe was due to the substrate material. The EDX-derived Ca/P ratio was found to be 1.34. This value is lower than that of stoichiometric hydroxyapatite (1.67), but as could be expected for nonstoichiometric apatites (see FTIR results). However, this value could also be indicative of a mixture of apatite with another calcium phosphate exhibiting a lower Ca/P

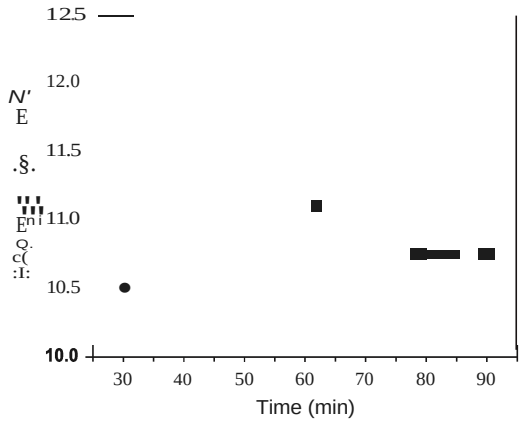

Figure 12. Variation of the mass of coating formed on TiN/316LSS versus duration of the polarization.

Table IY. Chemical composition of HAp coaling fonned on the TiN/316LSS substrate in the soluli.on containiJlg 3x 10-2 M Ca(NO,),, 1.8x 10-2 M .HzP04, 0.15 M NaNO, and 4% .Hz02 al 25 C, pH 4.5, with an applied potcntial -1.65 V/SCE for 45 minutes.

Element	O	Na	P	Cl	K	Ca	Tl	Cr	Fe
% weigbl	45.08	5.48	14.31	0.21	0.33	24.92	7.07	0.60	2.06
% atom	64.75	5.48	10.68	0.13	0.20	14.30	3.39	0.27	0.85

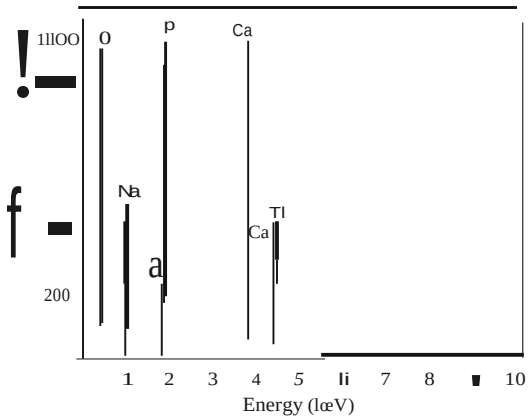

Figure 13. BOX spectrum of HAp coating formed on TiN/316LSS in the solution contain:ing 3 x 10-2 M Ca(NO,)z, 1.8 x 10-2 M mi.11zro•• 0.15 M $NaNO_3$ and 4% .$Hz0_2$ at 25 •C, pH 4.5, with an appli.cd potenlial -1.65 V/SCE for 45 minutes.

ratio, such as DCPD, although this phase was not detected by FfIR or XRD in our electrodeposition conditions.

4. CONCLUSION

In conclusion, we successfully obtained the formation of a HAp coating on TiN/316LSS. The effect of experimental conditions was investigated. The pH value of the solution, the H_20_2 concentration, the potential applied and the length of the experiments were found to have a direct impact on the coating features, in particular in terms of morphology (rod or needle, fialœ, spherical). Optimal conditions have been found: pH 4.5, applied potential -1.65 V/SCE, 4% H_20_2 and 45 minutes of electrodeposition process. The composition of the coatings obtained on TIN/316LSS was also analyzed. FfIR and EDX indicate that a nonstoichiometric apatite phase was obtained. XRD however indicat.es for some experimental conditions the formation of both DCPD and apatite. The results suggest that these conditions of electrodeposition on TiN-coated stainless steel are promising in view of the coating of bone implant with apatite.

Acknowledgments: This work was supported by the National Foundation for Science and Technology Development of Vietnam (under grant No. 104.03-2010.11, NAFOSTED), and was conducted within the context of the International Associated Laboratory *"Functional Composite Materials"* (LIA-FOCOMAT) created between the ITf (Vietnam)-VAST and the CIRIMAT (France)-CNRS institutes.

References and Notes

1. Y.L. Jeyachandran, Sa. K. Narayandass, D.Mangalaraj, C.Y.Bao, W.Li, Y. M. Llao, C.L. Zhang, L. Y. Xiao, and W. C. Chen, *Surf. Coat. TechnoL* 201, 3462 (2t06).
2. D. T.M.ThaDh, P.T.Nam, N.T.Phuong, L. X. Que, N. Van ADh, T. Hoang, and T. D, Lam, *Mater. Sei. Eng., C* 33, 2037 (2013).
3. M. M. Dewiàar, K. A. Kbalil, and J. K Lim, *Transactions of Nonferrous Metals Society of China* 17, 468 (2007).
4. D. J. Blackwood, *Corrosion Reviewer* 21, 97 (2003).
S. X. Liu, P.K. Chu. and C. Ding, *Materials Science and Engineering, R* 47, 49 (2004).
6. S.Bose and S. Tarafdc:r, *Acta Biomaterialia* 8, 1401(2012).
7. P.Harcuba, L. Bae6kové, J. StréskY, M. Baeâovâ, K. Novotnâ, and M. Janeœk, *J. Mech. Behav. Biomed. 1*, 96 (2012).
8. Z. Yuan-yuan, T.Jie, P.Ymg-chun, W. We, and W.Tao, *TIWIS.Nonferrous Met. Soc. China* 16, 633 (2t06).
9. A. Kar, K.S. Raja, and M. Misra, *Surf. Coat. TechnoL* 201, 3723 (2t06).
10. K.S. RajaT, M. Misra, and K. Paramguru. *Mater. Lett.* 59, 2137 (2005).
11. Y.Soda, H. Kawasaki, T. Ohshima, S. Nakashima, S. Kawame, and T.Toma, *Thin Solid Films* 506, 115 (2006).
12. A. *Visan*, D. Grossin, N. Stefan, L. Duta, F. M. Miroiu, G. E. Stan, M. Sopronyi, C. Luculescu, M. Freche, O. Marsan, C. Charvilat, S. Ciuca, and 1N. Mibailescu, *Mater. Sei. Eng., B* 185, 56 (2014).
13. Y.-P.Lu, M.-S.Li, S.-T. Li, Z.-G. Wang, and R.-F. Zhu, *Biomaterials* 25, 4393 (2004).
14. H. Wang, N. Eliaz, Z. Xiang, H.-P. Hsu, M. Spector, and L. W. Hobbs, *Biomaterials* 27, 4192 (2806).
15. 1. Demnati, D. Grossin, C. Combes, and C. Rey, *Journal of Medical and Biological Engineering* (2013) doi: 10.5405/jmbe.1459.
16. M. Yosbinari, Y. Ohtsuk:a, and T. Dérand, *Bionuuerials* 15, 529 (1994).
17. Y. L. Jeyacbandran, S. Venkatacbahun, B. Karunagaran, S. K. Narayandass, D. Mangalaraj, C. Y. Bao, and C. L. Zhang, *Mater. Sei. Eng., C* 27, 35 (2007).
18. C. Kean-Khoon, Sbarif Hussein Sbarif Zein, T. Soon Huat, and A. L. Ahmad, *Journal of Science and Technology* 49, 199 (2011).
19. Dong-Yang Lin and Xiao-Xiang Wang, *Surf. Coat. TechnoL* 204, 3205 (2010).
20. D. J. Blackwood and K. H. W. Seah, *Mater. Sei.E11g., C* 29, 1233 (2009).
21. D. T. M. ThaDh, P. T. Nam, H. T. Huong, N. T. Phuong,T. T. X. Hang, U. V.Vy, and T.Hoang, *J. Nanosci. NanotechnoL* 14, xxx (2014).
22. C. Rey, O. Marsan, C. Combes, C. Drouet, D.Grossin, and S.Sarda, Adwnces in Calcium Phosphate Biomaterials, edited by B. Ben-Nissan, Chaptec 8, Springer (2014), ISBN 978-3-642-53979-4.
23. J. Che:n, H. Iuang, and M. Hon, *J. Mater. Sei.: Mater. Med.* 9, 297 (1998).
24. X. Fan, J. Cben, J.-P. Zou, Q. Wan, Z.-C. Zhou, and J.-M. Ruan, *Traruactioru of Nonferrous Metal.! Society of China* 19, 347 (2009).
25. M. C. Kuo and S. K. Yen, *Mater. Sei. Eng., C* 20, 153 (2002).

26. C. Drouet, *BioMed Resœrch International* (2013), Volume 2013, Article ID 490946, 12 pages, doi: 10.1155/2013/490946.
'1:1. N. Vllldecanàelaere, C. Rey, and C. Drouet, *Journal of Materials Science: Materials in Medicine* 23, 2593 (2012).
28. M. Ma. W. Ye, and X.-X. Wang. *Mater. Lett.* 62, 3875 (2008).
29. K. ù:e, Y.-H. Jemig, Y.-M. Ko, H.-C. Choe, and W.A. Bnmtley, *Thin Solid Films* (2013), http:f/dx.doi.orgflO.lOl(i/j.bf.2013.09.002.
30. R. L. Watten, 2008 Calcium Hydroxyapatite (Certificate of Analysis, Standard Reference Materia1 2910a). (Gaithersburg, MD: Institute of Standards and Technology NIST Measurement Services Division National).
31. C.-H. Hou, C.-W. Chen, S.-M. Hou. Y.-T. Li, and F.-H. Lin, *Biomaterials* 30, 4700 (.2009).
32. Y.Wang and D. O. Northwood, *J. Power Sources* 165, 293 (2007).